NEUROSCIENCE

An isogenic panel of *App* knock-in mouse models: Profiling β-secretase inhibition and endosomal abnormalities

Naoto Watamura[1]†, Kaori Sato[1,2]†, Gen Shiihashi[3], Ayami Iwasaki[4], Naoko Kamano[1], Mika Takahashi[1], Misaki Sekiguchi[1], Naomi Mihira[1], Ryo Fujioka[1], Kenichi Nagata[5], Shoko Hashimoto[1], Takashi Saito[1,6], Toshio Ohshima[2], Takaomi C. Saido[1]*, Hiroki Sasaguri[1]*

We previously developed single App knock-in mouse models of Alzheimer's disease (AD) that harbor the Swedish and Beyreuther/Iberian mutations with or without the Arctic mutation (*App*$^{NL\text{-}G\text{-}F}$ and *App*$^{NL\text{-}F}$ mice). We have now generated *App* knock-in mice devoid of the Swedish mutations (*App*$^{G\text{-}F}$ mice) and evaluated its characteristics. Amyloid β peptide (Aβ) pathology was exhibited by *App*$^{G\text{-}F}$ mice from 6 to 8 months of age and was accompanied by neuroinflammation. Aβ-secretase inhibitor, verubecestat, attenuated Aβ production in *App*$^{G\text{-}F}$ mice, but not in *App*$^{NL\text{-}G\text{-}F}$ mice, indicating that the *App*$^{G\text{-}F}$ mice are more suitable for preclinical studies of β-secretase inhibition given that most patients with AD do not carry the Swedish mutations. Comparison of isogenic *App* knock-in lines revealed that multiple factors, including elevated C-terminal fragment β (CTF-β) and humanization of Aβ might influence endosomal alterations in vivo. Thus, experimental comparisons between different isogenic *App*, knock-in mouse lines will provide previously unidentified insights into our understanding of the etiology of AD.

INTRODUCTION

Alzheimer's disease (AD), the most prevalent cause of dementia, has been intensively investigated worldwide for more than 100 years since it was first reported (*1*). There are currently, however, no efficacious disease-modifying treatments available for AD, although aducanumab (*2*), an anti–amyloid β (Aβ) human monoclonal antibody, was approved for use by the U.S. Food and Drug Administration in June 2021 under the accelerated approval pathway. To date, substantial research advances have been achieved thanks to mouse models that recapitulate aspects of the AD pathophysiology seen in humans. Most AD mouse models overexpress mutant amyloid precursor protein (APP) or APP/presenilin 1 (PS1) complementary DNAs inserted into unknown loci of the host animals, which causes artificial aspects of their complex phenotypes (*3*). We previously developed *App*$^{NL\text{-}F}$ and *App*$^{NL\text{-}G\text{-}F}$ knock-in (KI) mice that harbor the Swedish (KM670/671NL) and Beyreuther/Iberian (I716F) mutations—with or without the Arctic (E693G) mutation—that do not depend on APP or APP/PS1 overexpression for their pathophysiological phenotype. These *App*-KI mice exhibit age-dependent neuritic plaques composed of Aβ peptide in the brain, followed by gliosis and memory impairment (*4*).

It should be noted, however, that the Swedish mutations, located adjacent to the cleavage site of APP by β-secretase, results in a drastic increase in CTF-β (C-terminal fragment β) levels and influences the in vitro APP processing efficacy of β-secretase β-site Amyloid precursor protein Cleaving Enzyme 1 (BACE1) inhibitors (*5*). The presence of Swedish mutations therefore renders the *App*$^{NL\text{-}F}$ and *App*$^{NL\text{-}G\text{-}F}$ lines as unsuitable for preclinical studies of β-secretase inhibitors. In effect, Swedish mutations are present in most APP transgenic mouse models that overexpress APP, and moreover, there is no single *App*-KI mouse model that recapitulates amyloid pathology in the brain in the absence of Swedish mutations. In addition, CTF-β itself has been reported to have toxic effects such as early endosomal dysfunction (*6*, *7*). On the basis of these facts, we thought that *App*-KI mice without the Swedish mutations would be a valuable model for AD research.

In this study, we used a CRISPR-Cas9 system to develop *App*$^{G\text{-}F/G\text{-}F}$-KI (*App*$^{G\text{-}F}$) mice harboring the Arctic and Beyreuther/Iberian mutations but devoid of the Swedish mutations (*8*, *9*). Similar to the *App*$^{NL\text{-}F}$ and *App*$^{NL\text{-}G\text{-}F}$ lines, the *App*$^{G\text{-}F}$ line showed an age-dependent amyloid pathology, neuroinflammation, and synaptic alteration. Acute administration of verubecestat (*10*, *11*), a potent selective BACE1 inhibitor, reduced Aβ levels in *App*$^{G\text{-}F}$ mice but not in *App*$^{NL\text{-}G\text{-}F}$ mice. We also found that early endosomal alteration was present in the brains of all the *App*-KI lines including *App*$^{G\text{-}F}$ mice and *App*-KI mice with only the humanized Aβ sequence (*App*$^{huA\beta}$ mice). Our findings demonstrate that BACE1 activity can be appropriately evaluated in *App*$^{G\text{-}F}$ mice without the interference of the Swedish mutations and that endosome alterations are not exclusively caused by elevated CTF-β or Aβ levels in vivo.

RESULTS

Generation of *App*$^{G\text{-}F}$ and *App*^{huA}β mice by CRISPR-Cas9

We previously developed *App*$^{NL\text{-}G\text{-}F}$ mice by manipulation of the mouse *App* gene using a KI strategy (*4*). Exon 16 of the *App* gene contains the Swedish mutations (KM670/671NL), while exon 17 contains the Arctic and Beyreuther/Iberian mutations (Fig. 1A). First, single-guide RNA (sgRNA)–App-Exon16 and single-stranded

[1]Laboratory for Proteolytic Neuroscience, RIKEN Center for Brain Science, 2-1 Hirosawa, Wako, Saitama 351-0198, Japan. [2]Laboratory for Molecular Brain Science, Department of Life Science and Medical Bioscience, Waseda University, Shinjuku, Tokyo 162-8480, Japan. [3]Neurological Institute, Shonan Keiiku Hospital, 4360 Endo, Fujisawa, Kanagawa 252-0816, Japan. [4]Yamaguchi University School of Medicine, 1-1-1 Minamikogushi, Ube, Yamaguchi 755-8505, Japan. [5]Department of Functional Anatomy and Neuroscience, Nagoya University Graduate School of Medicine, Nagoya, Aichi 466-8550, Japan. [6]Department of Neurocognitive Science, Institute of Brain Science, Nagoya City University Graduate School of Medical Sciences, Nagoya, Aichi 467-8601, Japan.
*Corresponding author. Email: takaomi.saido@riken.jp (T.C.S.); hiroki.sasaguri@riken.jp (H.S.)
†These authors contributed equally to this work.

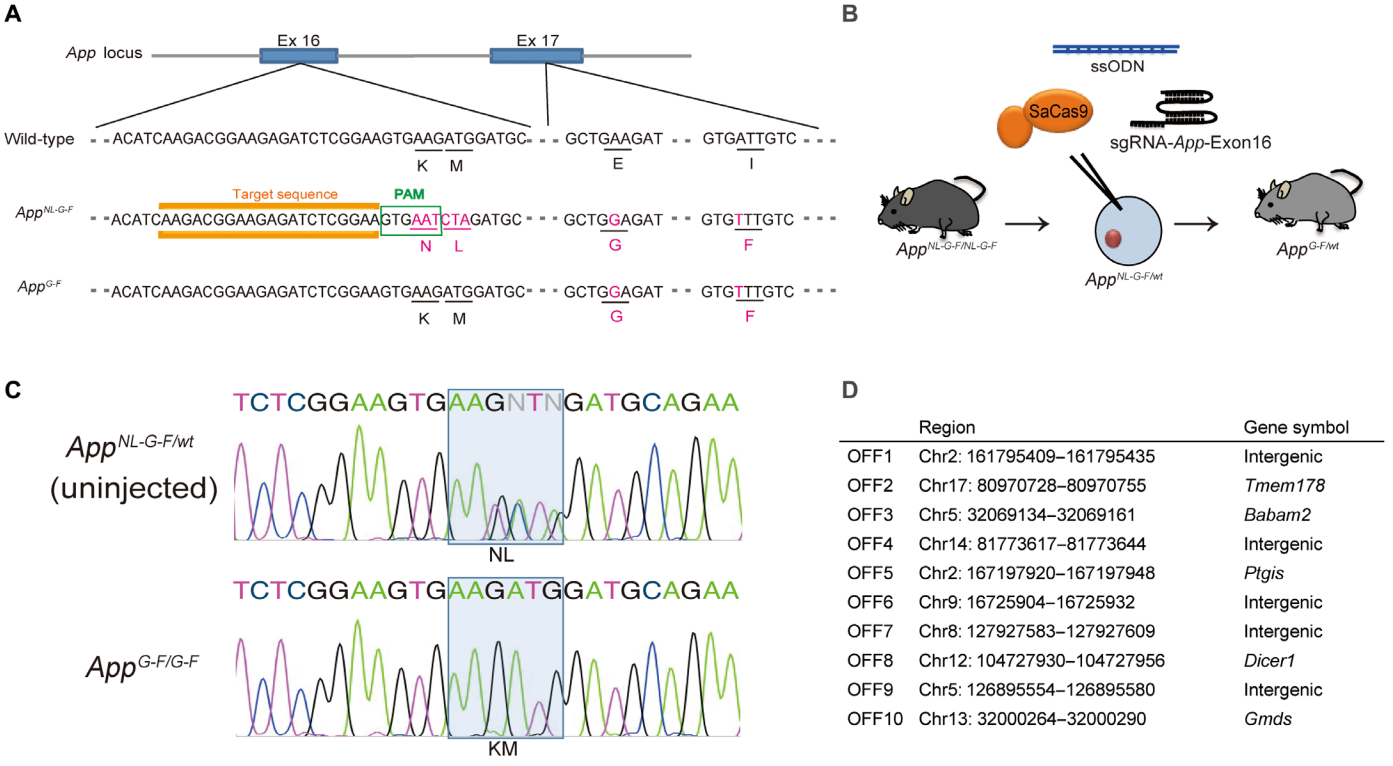

	Region	Gene symbol
OFF1	Chr2: 161795409–161795435	Intergenic
OFF2	Chr17: 80970728–80970755	*Tmem178*
OFF3	Chr5: 32069134–32069161	*Babam2*
OFF4	Chr14: 81773617–81773644	Intergenic
OFF5	Chr2: 167197920–167197948	*Ptgis*
OFF6	Chr9: 16725904–16725932	Intergenic
OFF7	Chr8: 127927583–127927609	Intergenic
OFF8	Chr12: 104727930–104727956	*Dicer1*
OFF9	Chr5: 126895554–126895580	Intergenic
OFF10	Chr13: 32000264–32000290	*Gmds*

Fig. 1. Generation of the single *App*$^{G\text{-}F}$-KI mice. (**A**) Exact sequences showing sgRNA (orange) with the PAM site (green) in the mouse *App* gene. Red characters represent the Swedish (KM670/671NL), Arctic (E693G), and Beyreuther/Iberian (I716F) mutations, respectively. (**B**) Schematic illustration of CRISPR-Cas9–mediated genome editing in *App*$^{NL\text{-}G\text{-}F}$-KI mouse zygotes by microinjection. (**C**) Sanger sequencing results determined *App*$^{NL\text{-}G\text{-}F/wt}$ (top) and *App*$^{G\text{-}F/G\text{-}F}$ genotype (bottom). The desired mutation loci (NL670/671KM) are indicated as a rectangular shape in blue shading. See also fig. S1. (**D**) Regional information of potential off-target sites that were identified using Cas-OFFinder (www.rgenome.net/cas-offinder/) and COSMID (https://crispr.bme.gatech.edu/).

oligodeoxynucleotide (ssODN) containing the wild-type (WT) sequence to substitute the Swedish mutations (NL670/671KM) together with *Staphylococcus aureus* Cas9 (SaCas9) mRNA, where the protospacer adjacent motif (PAM) sequence is required as NNGRRT, were injected into the cytoplasm of heterozygous zygotes of *App*$^{NL\text{-}G\text{-}F}$ mice. The PAM sequence overlapped with the Swedish mutations so that, when KI of the WT sequence occurred, it could prevent sequential cleavages by SaCas9 because the original PAM site had disappeared (Fig. 1, A and B). Sanger sequencing analysis revealed that the desired substitution via homology-directed repair occurred successfully in the *App*$^{NL\text{-}G\text{-}F}$ allele of the founder mice with an efficiency of 10.8% (Fig. 1C). Crossing the founder mice with WT mice to generate F1 mice, we confirmed that the Swedish mutations were fully removed from the *App*$^{NL\text{-}G\text{-}F}$ allele (Fig. 1C). Using an identical strategy in *App*^{NL} zygotes (see Materials and Methods), we also generated *App*$^{huA\beta}$ mice that carry only the humanized Aβ sequence in the mouse *App* gene without any familial AD-causing mutation. We confirmed that there were no unexpected mutations in exons 16, 17, and 18 of the *App* gene in *App*$^{G\text{-}F}$ and *App*$^{huA\beta}$ mice and others (fig. S1), indicating that all these lines are isogenic. *App*$^{G\text{-}F/wt}$ mice were then intercrossed to obtain homozygous *App*$^{G\text{-}F/G\text{-}F}$ mice that were viable. To explore the off-target effects of CRISPR-Cas9–mediated genome editing in the founder mice, we searched for potential off-target sites using the online tool COSMID (*12*) and Cas-OFFinder (*13*) (Fig. 1D). Targeted sequencing analysis focusing on the candidate genomic regions revealed that no off-target modification took place in the founder mice of *App*$^{G\text{-}F}$ and *App*$^{huA\beta}$ mice.

Neuropathology of *App*$^{G\text{-}F}$ mice

We next analyzed the extent of amyloid pathology in the *App*$^{G\text{-}F}$ mice. $A\beta_{42}$ levels in the cortex were age-dependently increased in the tris-HCl– and guanidine-HCl (GuHCl)–soluble fractions, with $A\beta_{40}$ levels remaining relatively stable (Fig. 2, A and B). We also observed that progressive amyloid pathology mainly in the cortex and hippocampus occurred in an age-dependent manner (Fig. 2, C and D). Initial deposition of Aβ was observed around 4 months of age in the *App*$^{G\text{-}F}$ mice. At 12 months, Aβ deposition in the brains of *App*$^{G\text{-}F}$ mice detected in a much larger area than that in the *App*$^{NL\text{-}F}$ mice but at a lower level to that in *App*$^{NL\text{-}G\text{-}F}$ mice (fig. S2). In addition, we analyzed the Aβ species constituting amyloid plaques in the *App*$^{G\text{-}F}$ mice using N-terminal, C-terminal ($A\beta_{40}$ and $A\beta_{42}$), and $A\beta_{3(pE)\text{–}X}$ [pE (pyroglutamate] specific antibodies. $A\beta_{40}$, $A\beta_{42}$, and $A\beta_{3(pE)\text{–}X}$ species were detected in the brain with a predominant deposition of $A\beta_{42}$ over $A\beta_{40}$ (Fig. 2E). These results are consistent with the neuropathology observed in patients with sporadic AD and in *App*$^{NL\text{-}F}$and *App*$^{NL\text{-}G\text{-}F}$ mice (*4*).

Chronic inflammation surrounding Aβ plaques in the brain is a pathological hallmark of AD. We therefore investigated the status of glial cells surrounding amyloid plaques in the *App*$^{G\text{-}F}$ mice. Reactive astrocyte and activated microglia are pathological signs of neuroinflammation, with evidence of both being observed (Fig. 2F). We also examined pre- and postsynaptic alterations in brain slices and detected loss of synaptophysin and postsynaptic density protein 95 immunoreactivity near the Aβ plaques, which is consistent with those in other *App*-KI mice (Fig. 2G) (*4*).

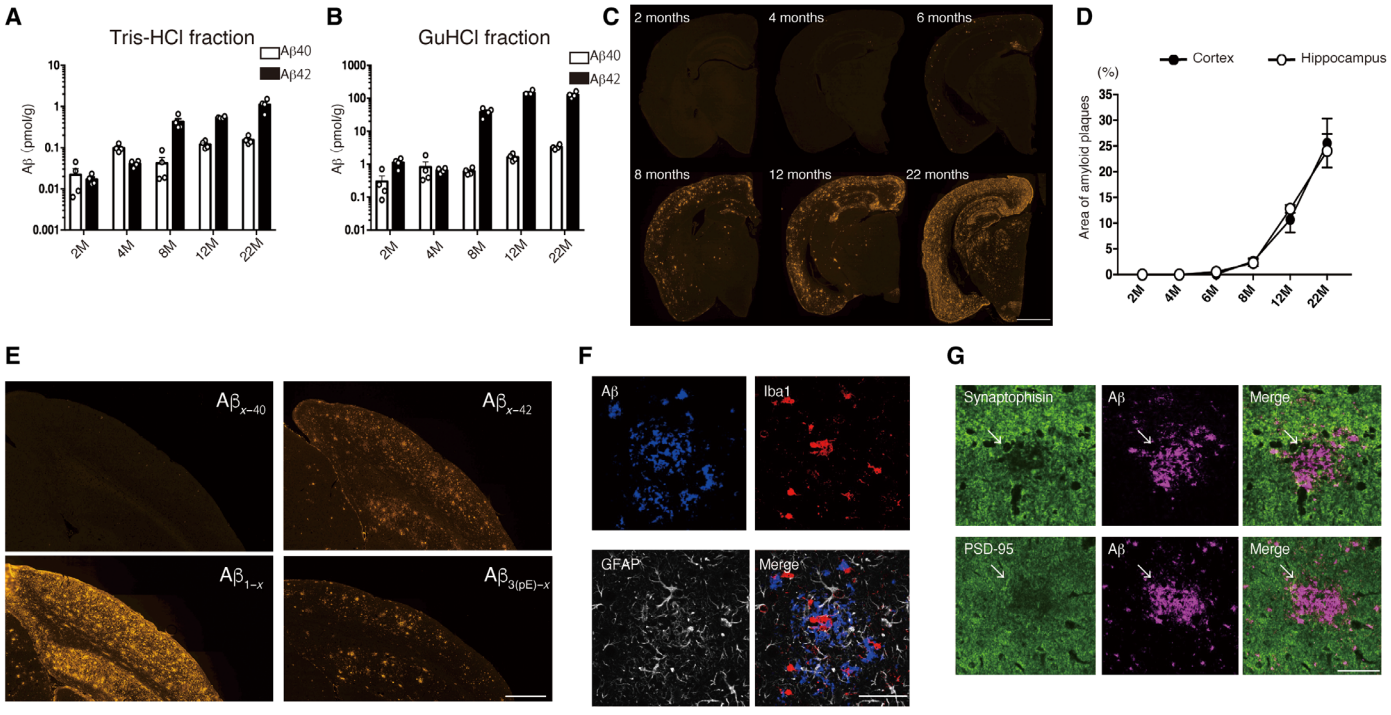

Fig. 2. Neuropathology of *App*$^{G\text{-}F}$ mice. (**A** and **B**) Aβ content detected by enzyme-linked immunosorbent assay (ELISA) using tris-HCl–soluble fraction (A) and GuHCl-soluble fraction (B) of the cortices of *App*$^{G\text{-}F}$ mice at 2, 4, 8, 12, and 22 months (M) ($n = 4$ at each time point). Each bar represents the mean ± SEM. (**C**) Immunohistochemistry images showing Aβ deposition as indicated by immunostaining with N1D antibody against $Aβ_{1–5}$. Scale bar, 1 mm. (**D**) Quantitative analysis of amyloid plaque areas in the cortices and hippocampi of *App*$^{G\text{-}F}$ mice at 2, 4, 8, and 12 months ($n = 4$ at each time point) and at 22 months ($n = 3$). Each bar represents the mean ± SEM. (**E**) Specific antibodies against N terminus [$Aβ_{1–x}$ and $Aβ_{3(pE)–x}$] and C terminus ($Aβ_{x–40}$ and $Aβ_{x–42}$) of Aβ reveal the deposition of each species of Aβ in the brains of 22-month-old *App*$^{G\text{-}F}$ mice. Scale bar, 500 μm. (**F**) Inflammatory responses in the cortices of *App*$^{G\text{-}F}$ mice at 22 months. Astrocytes (gray) and microglia (red) can be seen surrounding Aβ (blue), as detected by triple staining with antibodies against glial fibrillary acidic protein (GFAP), ionized calcium-binding adapter molecule 1 (iba1), and the N terminus of human Aβ (82E1), respectively. Scale bar, 100 μm. (**G**) Synaptic alteration detected in the hippocampus of a 22-month-old *App*$^{G\text{-}F}$ mouse. Aβ detected by 4G8 antibody against $Aβ_{17–24}$ was double stained with synaptophysin antibody as a presynaptic marker or with postsynaptic density protein 95 (PSD-95) antibody as a postsynaptic marker. White arrows indicate synaptic loss near Aβ aggregation. Scale bar, 25 μm.

Assessment of BACE1 inhibition in *App*$^{G\text{-}F}$ mice

The Swedish mutations have been considered to underlie the decreased APP processing potency of β-secretase inhibitors. Previous studies have shown that β-secretase inhibition is less efficacious in cells stably overexpressing the *APP*-containing Swedish mutations than from cells transfected with WT APP (*14*, *15*). To compare the potency of β-secretase inhibition in animal models—with or without Swedish mutations in the *APP* gene—not relying on the overexpression paradigm, we administrated verubecestat, a potent BACE1 inhibitor, to 3-month-old WT, *App*$^{NL\text{-}G\text{-}F}$, and *App*$^{G\text{-}F}$ mice following a previously reported experimental protocol (*11*). We found that a single oral administration of verubecestat at the dose of 10 mg/kg significantly reduced both $Aβ_{40}$ and $Aβ_{42}$ levels in the cortices of *App*$^{G\text{-}F}$ mice, but not in *App*$^{NL\text{-}G\text{-}F}$ mice, 3 hours after treatment (Fig. 3, A to D). These results indicate that the Swedish mutations are responsible for the poor potency of BACE1 inhibitors in vivo and that *App*$^{G\text{-}F}$ mice could serve as a powerful tool for the precise characterization of BACE1 and candidate inhibitory compounds.

Relationship between the quantity of CTF-β and endosomal abnormality in vivo

Several studies have reported that the Swedish mutations alter the APP processing and shift the processing toward an amyloidogenic pathway via a competitive behavior between α- and β-secretases (*5*, *16*). In an earlier study, we showed that the ratio of CTF-β/α levels in *App*$^{NL\text{-}F}$ and *App*$^{NL\text{-}G\text{-}F}$ mice is higher than that in WT mice (*4*). Here, we used five different isogenic *App*-KI lines and WT mice to examine the effect of the mutations on the quantity of CTF-β and the extent of endosomal alteration (Table 1). The ratio of CTF-β/α in *App*$^{G\text{-}F}$ mice was much lower compared to *App*^{NL}, *App*$^{NL\text{-}F}$, and *App*$^{NL\text{-}G\text{-}F}$ mice with no alteration of APP levels (figs. S3 and S4). The quantity of CTF-β in the brains of *App*$^{G\text{-}F}$ mice was comparable to those of *App*^{huAβ} mice and significantly lower compared to other *App*-KI lines that harbor the Swedish mutations (Fig. 4, A and B, and fig. S4E). However, when we compared the quantity of CTF-β among WT, *App*^{huAβ}, and *App*$^{G\text{-}F}$ mice, the latter two showed significant increase of CTF-β, indicating that humanization of Aβ influenced APP processing in vivo (figs. S3G and S4H). We next examined whether CTF-β affects endosomal appearance in vivo (Fig. 4, C to E, and fig. S5). Some groups suggest that accumulated CTF-β itself induces endosome abnormalities independent of Aβ toxicity in vitro (*6*, *7*). We focused on early endosomal antigen 1 (EEA1) as an early endosome marker and performed immunohistochemical analyses of the hippocampal CA1 region in six mouse lines: WT, *App*^{huAβ}, *App*^{NL}, *App*$^{NL\text{-}F}$, *App*$^{G\text{-}F}$, and *App*$^{NL\text{-}G\text{-}F}$-KI mice. We detected a significant increase in the mean EEA1^{+} area in the CA1 pyramidal cell layer of five mutant lines compared with that of WT mice (Fig. 4, C and D). We consistently observed a significant alteration of the distribution of endosome size in the five mutant mouse lines, including *App*^{huAβ}-KI mice, compared with that of WT mice (Fig. 4E). This was seen as an increase in the ratio of larger endosomes (>1 μm^2) and a

decrease in the ratio of smaller endosomes (<0.5 μm^2) (Fig. 4E). Notably, endosomal sizes were enlarged in the brains of $App^{G\text{-}F}$ and $App^{huA\beta}$ mice, the extent of which was similarly observed in $App^{NL\text{-}G\text{-}F}$ mice irrespective of large differences in CTF-β levels (Fig. 4, B and D). Unexpectedly, endosome enlargement was most significant in $App^{huA\beta}$ mice (fig. S5B). These findings suggest that multiple factors such as CTF-β–dependent, Aβ-dependent, and APP-independent pathways may influence endosomal alterations in vivo.

DISCUSSION

In the present study, by removing the Swedish mutation from $App^{NL\text{-}G\text{-}F}$ mice, we developed a new *App*-KI line, $App^{G\text{-}F}$, which harbors both the Arctic and Beyreuther/Iberian mutations. The $App^{G\text{-}F}$ mice exhibited an age-dependent and typical amyloid pathology, neuroinflammation, characterized by reactive astrocytes and activated microglia surrounding the Aβ plaques, and aberrant pre- and postsynaptic structures near the plaques. Verubecestat intervention effectively reduced Aβ levels in the cortices of $App^{G\text{-}F}$ mice but not in the conventional *App*-KI mice containing the Swedish mutation. Endosomal alteration was also observed in all the *App*-KI lines including $App^{G\text{-}F}$ mice and $App^{huA\beta}$ mice despite relatively low level of CTF-β in these two lines.

Aβ deposition in the brains of $App^{G\text{-}F}$ mice occurs from around 4 months of age, compared to around 2 months of age in $App^{NL\text{-}G\text{-}F}$ mice and 6 months in $App^{NL\text{-}F}$ mice (*4*), suggesting that the $App^{G\text{-}F}$ mice serve as "a moderate model" of the three lines from the point of view of amyloidosis in the mouse brain (fig. S2). $App^{G\text{-}F}$ mice also showed an age-dependent amyloid pathology in the subcortical area as well as in the cortex and hippocampus, which is consistent with human carriers of the Arctic mutation (*17*). This is the first AD mouse model that recapitulates amyloid pathology in the brain but does not harbor the Swedish mutation and is not dependent on APP overexpression.

Previous studies based on transgenic mice overexpressing the *APP* gene with familial mutations and CRISPR-Cas9–mediated genomic modified iPSCs (induced pluripotent stem cells) indicated that AD-associated early endosomal enlargement depends on the excess accumulation of CTF-β but not Aβ (*6*, *7*, *18*–*22*). Endosome enlargement may manifest as the disturbances of endocytic signaling

Table 1. Mouse lines used in the present study.

1. WT (C57BL/6J)
2. $App^{huA\beta}$ line (*App*-KI mice with Aβ sequence humanized)
3. App^{NL} line (*App*-KI mice carrying Swedish mutations)
4. $App^{NL\text{-}F}$ line (*App*-KI mice carrying Swedish and Iberian mutations)
5. $App^{G\text{-}F}$ line (*App*-KI mice carrying Arctic and Iberian mutations)
6. $App^{NL\text{-}G\text{-}F}$ line (*App*-KI mice carrying Swedish, Arctic, and Iberian mutations)

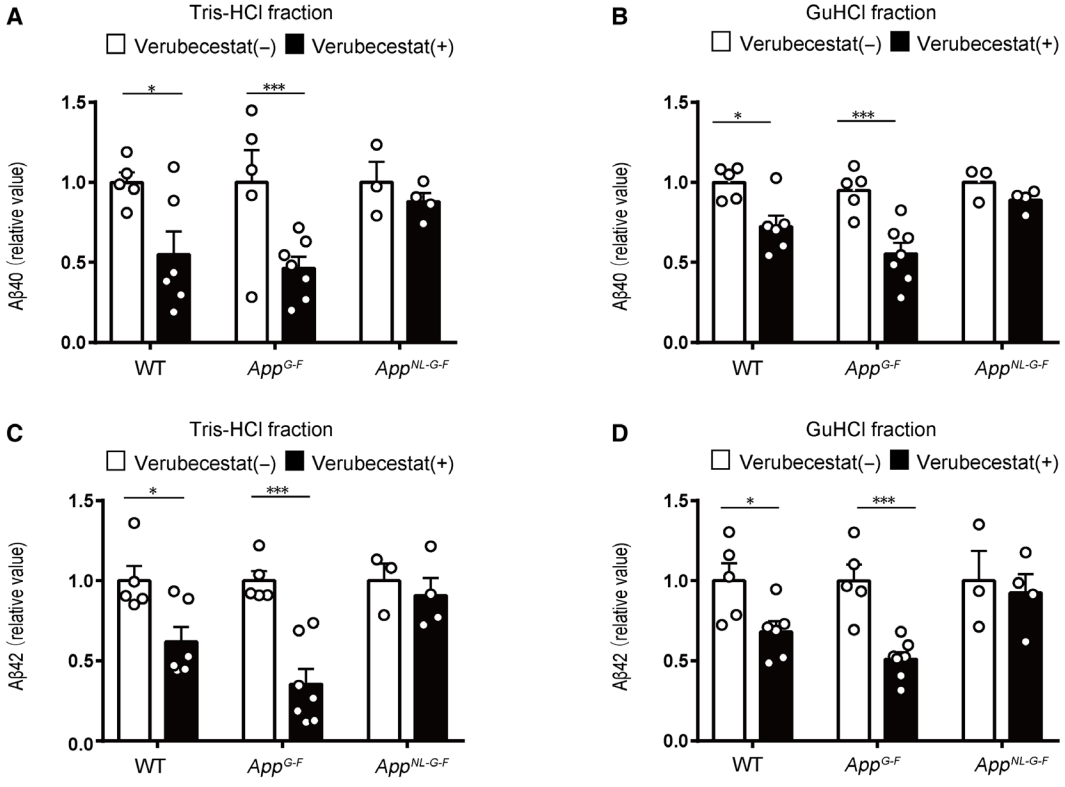

Fig. 3. Removal of the Swedish mutations rescues the BACE1 inhibitory effect of verubecestat. (**A** to **D**) $A\beta_{40}$ and $A\beta_{42}$ levels detected by ELISA were decreased both in the tris-HCl fraction (A and C) and GuHCl fraction (B and D) of 3-month-old WT and $App^{G\text{-}F}$ mice but not in $App^{NL\text{-}G\text{-}F}$ mice. Each bar represents the mean ± SEM. *$P < 0.05$ and ***$P < 0.001$ [WT: verubecestat(+), $n = 5$; verubecestat(−), $n = 6$. $App^{G\text{-}F}$: verubecestat(+), $n = 5$; verubecestat(−), $n = 7$. $App^{NL\text{-}G\text{-}F}$: verubecestat(+), $n = 3$; verubecestat(−), $n = 4$. Student's *t* test].

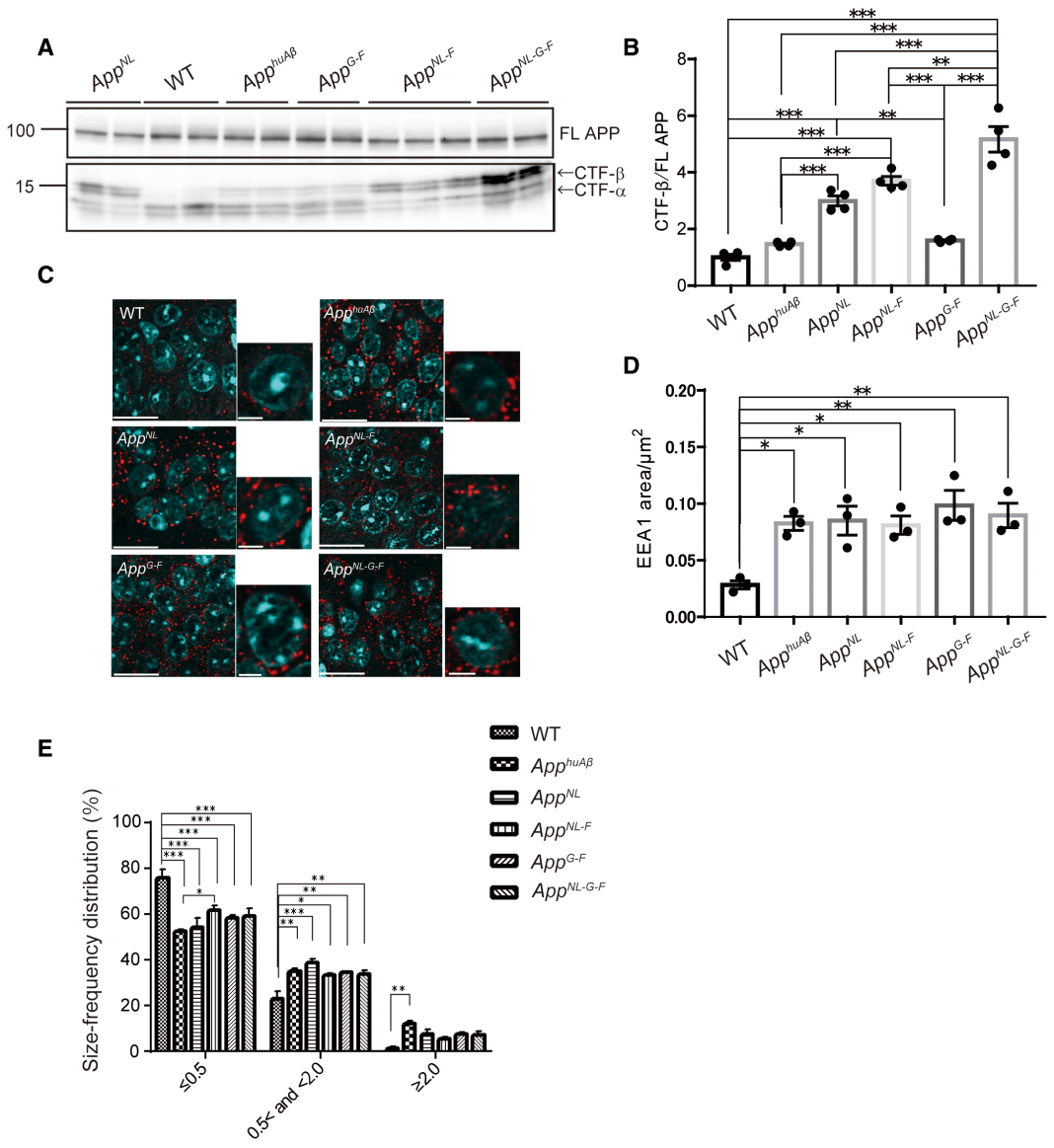

Fig. 4. APP CTF expression levels and endosome abnormalities. (**A**) APP CTF expression in the hippocampi of 12-month-old WT, $App^{huA\beta}$, App^{NL}, App^{NL-F}, App^{G-F}, and App^{NL-G-F} mice. See also figs. S3 and S4. FL, full-length. (**B**) Quantification of relative levels of APP CTF-β using within-lane normalization to full-length APP before normalizing to WT. WT, $App^{huA\beta}$, App^{NL}, App^{NL-F}, App^{G-F}, and App^{NL-G-F}; $n = 4$ for each genotype, one-way analysis of variance (ANOVA) followed by Tukey's multiple comparisons test. (**C**) Immunohistochemical images of early endosomes in CA1 pyramidal cells detected by EEA1 antibody (red) and Hoechst33342 staining of nuclei (blue). Brain sections from 12-month-old WT, $App^{huA\beta}$, App^{NL}, App^{NL-F}, App^{G-F}, and App^{NL-G-F} mice. Scale bars, 20 μm (left) and 5 μm (right), respectively, for each genotype. (**D**) Statistical analysis of $EEA1^+$ area per square micrometer in pyramidal cells of hippocampal CA1 region. (**E**) Endosomal size distribution was statistically analyzed using MetaMorph imaging software. WT, $App^{huA\beta}$, App^{NL}, App^{NL-F}, App^{G-F}, and App^{NL-G-F}; $n = 3$ for each genotype, one-way ANOVA followed by Tukey's multiple comparisons test (D and E). Each bar represents the mean ± SEM. $^*P < 0.05$, $^{**}P < 0.01$, and $^{***}P < 0.001$ (B, D, and E).

at the earliest stage of AD (*23*). On the other hand, other studies have reported that Aβ toxicity is indeed a causative factor for impaired endocytic sorting (*24*–*26*). In this study, using an isogenic panel of *App*-KI mouse lines, we observed early endosomal alterations in hippocampal CA1 pyramidal neurons of *App*-KI lines compared to WT mice (Fig. 4 and fig. S5). Our results show that humanization of Aβ alone induces endosomal enlargement in mice. *Eea1* was identified as one of hub genes in a module that was down-regulated in another humanized Aβ KI mouse by using weighed gene coexpression network analysis [see figure 7c in (*27*)]. Although involvement of endosomal function in this analysis was not clear, it is possible that endosomal alteration is a common phenomenon in humanized Aβ KI mice. On the other hand, recent studies indicate that endosomal enlargement occurs via an APP-independent pathway (*28*, *29*). Together, endosomal alteration associated with AD cytopathogenesis may occur via different means such as CTF-β–dependent, Aβ-dependent, and APP-independent pathways. Further analyses are required to assess whether these alterations observed in our models affect endosomal functions in vivo.

A large number of BACE1 inhibitors have been explored and investigated as potent disease-modifying drugs in the AD research

field, but all of them, to our knowledge, have failed to show efficacy in clinical trials. However, as the A673T (Icelandic) mutation (*30*) positively established the proof of concept that the inhibition of β-secretase cleavage reduces the risk of AD onset, the discovery of BACE1 inhibitory compounds that pass through the blood-brain barrier and directly abrogate Aβ production in human brains remains a promising path to treat patients with AD. Although single $App^{NL\text{-}F}$ and $App^{NL\text{-}G\text{-}F}$-KI mice have been used in more than 500 laboratories and pharmaceutical companies worldwide as second-generation mouse models of AD (*4*), these mice are not compatible with BACE1-related studies because of the presence of Swedish mutations. Our results provide consistent evidence that the Swedish mutations hinder the BACE1 inhibitory activities of verubecestat in vivo, similar to several reports showing the reduced activity of BACE1 inhibitors including not just verubecestat (*14*) but also other drug candidates in mice harboring the Swedish mutations (*16*, *31*). Thus, $App^{G\text{-}F}$ mice now profile as a novel type of single *App*-KI mice without the interference of the Swedish mutations. The potential exists for these mice to be used efficiently and precisely to identify active compounds for BACE1 inhibition in vivo that might have been overlooked in a vast number of studies in which AD model mice were used that contained the Swedish mutations and were based on an APP overexpression paradigm. Our range of single *App*-KI mice, including the $App^{NL\text{-}F}$, $App^{NL\text{-}G\text{-}F}$, and $App^{G\text{-}F}$ lines, is available for use by research groups and companies worldwide that can choose the AD mouse model line most suited to the purpose of their study.

MATERIALS AND METHODS

Mice

All animal experiments were conducted in compliance with the regulations stipulated by the RIKEN Center for Brain Science. $App^{NL\text{-}F}$ or $App^{NL\text{-}G\text{-}F}$ mice expressing two or three familial AD mutations [Swedish (KM670/671NL) and Beyreuther/Iberian (I716F) with or without the Arctic (E693G) mutation] driven by the endogenous promoter, as well as the humanized Aβ sequence, were generated described previously (*4*). $App^{NL\text{-}G\text{-}F}$ and ICR mice were used as zygote donors and foster mothers. C57BL/6J and App^{NL} mice were prepared as controls (*4*). All mutant mice used in this study were homozygous for the expressed mutations. Both male and female mice were used in our experiments. All mice were bred and maintained in accordance with the regulations for animal experiments promulgated by the RIKEN Center for Brain Science.

Generation of $App^{G\text{-}F}$ mice

sgRNA targeting mouse *App* exon 16 was designed in silico using the CRISPR design tool (*32*). To reduce the possibility of off-target events, SaCas9 that recognizes NNGRRT as the PAM site was selected to introduce double-stranded breaks. ssODN was designed to cause NL670/671KM substitution (AATCTA>AAGATG) overlapping the PAM region so that the oligonucleotide did not include silent mutations, thus preventing rebinding and recutting after the desired genome modification via homology-directed repair. A plasmid vector (Addgene, no. 61591) was used for in vitro transcription of SaCas9 mRNA, and sgRNA was synthesized as described previously (*33*). Information on the primers and oligonucleotides used for the in vitro synthesis of CRISPR tools is listed in table S1. The prepared SaCas9 mRNA (100 ng/μl) and sgRNA (100 ng/μl) along with ssODN (100 ng/μl) were coinjected into the cytoplasm of $App^{NL\text{-}G\text{-}F/wt}$ zygotes. Founder mice were identified by polymerase chain reaction (PCR) and sequencing analysis of the targeted site and crossed with WT mice to obtain heterozygous F1 mice.

Generation of $App^{huA\beta}$ mice

To generate $App^{huA\beta}$ mice that carried only the humanized Aβ sequence, virtually, the same strategy was used to that used for developing $App^{G\text{-}F}$ mice. The prepared sgRNA, mRNA, and ssODN were identical to those used for $App^{G\text{-}F}$ mice, with the only difference being that App^{NL} zygotes instead of $App^{NL\text{-}G\text{-}F}$ zygotes were used for injecting genome editing tools. Potential off-target sites were also identical as those for $App^{G\text{-}F}$ mice.

Off-target effects analysis

Candidate sequences were identified in silico using COSMID (https://crispr.bme.gatech.edu/) (*12*) and Cas-OFFinder (www.rgenome.net/cas-offinder/) (*13*), allowing up to 3–base pair (bp) mismatches and 1-bp DNA and/or RNA bulge. Genomic DNA extracted from mouse tails was amplified by PCR with the primers listed in table S2. All genomic sequences of the amplicons were analyzed by Sanger sequencing using a DNA sequencer (ABI 3730xl).

Genotyping

Genomic DNA was extracted from mouse tails in lysis buffer [10 mM tris-HCl (pH 8.5), 5 mM EDTA (pH 8.0), 0.2% SDS, 200 mM NaCl, and proteinase K (20 μg/ml)] through a process of ethanol precipitation. To distinguish *App*-KI lines including $App^{huA\beta}$ and $App^{G\text{-}F}$ mice from WT mice, purified DNA was subjected to PCR and followed either by Sanger sequencing analysis or by digestion with EcilI (New England BioLabs, R0590) at 37°C for 1 hour. Genotyping primers for *App*-KI mice are listed in table S2.

Western blotting

Mouse brain tissues were homogenized in lysis buffer containing 50 mM tris (pH 7.6), 0.15 M NaCl, 1% Triton X-100, and cOmplete protease inhibitor cocktail (Roche Diagnostics) using a Multi-beads Shocker (Yasui Kikai). Homogenates were incubated at 4°C for 1 hour and centrifuged at 15,000 rpm for 30 min, and the supernatants were collected as loading samples. Concentrations of protein samples were measured with the aid of a bicinchoninic acid protein assay kit (Thermo Fisher Scientific). Equal amounts of proteins were subjected to SDS–polyacrylamide gel electrophoresis and transferred to polyvinylidene difluoride membranes. For detection of APP-CTFs, delipidated samples were loaded onto membranes and boiled for 5 min in phosphate-buffered saline (PBS) before blocking with enhanced chemiluminesence (ECL) primer blocking buffer (GE Healthcare). Membranes were incubated at 4°C with primary antibodies against APP (MAB348, Millipore; 1:2000) or APP-CTFs (A8717, Sigma-Aldrich; 1:1000) with glyceraldehyde-3-phosphate dehydrogenase (HRP-60004, Proteintech; 1:150,000) as a loading control. Targeted proteins were visualized with ECL select (GE Healthcare) and a LAS-3000 Mini Lumino image analyzer (Fujifilm).

Immunohistochemistry

Paraffin-embedded mouse brains were sectioned (thickness, 4 μm) and subjected to deparaffinization processing; antigen retrieval was then performed by autoclaving at 121°C for 5 min. Brain sections were treated with 0.3% H_2O_2 in methanol solution for 30 min to inactivate endogenous peroxidases. Sections were rinsed with TNT

buffer [0.1 M tris (pH 7.5), 0.15 M NaCl, and 0.05% Tween 20], blocked using a TSA Biotin System kit and incubated at 4°C overnight with primary antibodies diluted in TNB buffer [0.1 M tris (pH 7.5), 0.15 M NaCl]. Primary antibody dilution ratios are listed in table S3. Sections were washed and incubated with biotinylated secondary antibody, and a tyramide signal amplification system was used to detect amyloid pathology. For detection of neuroinflammatory signs and early endosome pathology, secondary antibodies conjugated with Alexa Fluor 555 diluted in TNB buffer or 0.2% casein in PBS were used. Sections were stained for 15 min with Hoechst33342 (Thermo Fisher Scientific) diluted in PBS and then mounted with PermaFluor (Thermo Fisher Scientific). Section images were obtained using a confocal laser scanning microscope FV-1000 (Olympus) and a NanoZoomer Digital Pathology C9600 (Hamamatsu Photonics). Quantification of immunoreactive signals was performed using Metamorph Imaging Software (Molecular Devices) and Definiens Tissue Studio (Definiens).

Enzyme-linked immunosorbent assay

Mouse brain samples were homogenized in lysis buffer [50 mM tris-HCl (pH 7.6), 150 mM NaCl, and protease inhibitor cocktail] using a Multi-beads shocker (Yasui Kikai, Japan). The homogenates were centrifuged at 70,000 rpm at 4°C for 20 min, and the supernatant was collected as a tris-soluble (TS) fraction to which 1/11 (v/v) of 6 M GuHCl in 50 mM tris and protease inhibitors were added. The pellet was loosened in lysis buffer with a Pellet Pestle (KIMBLE), dissolved in 6 M GuHCl buffer, and sonicated at 25°C for 1 min. The sample was incubated for 1 hour at room temperature and then subjected to centrifugation at 70,000 rpm at 25°C for 20 min. The supernatant was collected as a GuHCl-soluble fraction. TS and GuHCl-soluble fractions were applied to 96-well plates using an Aβ ELISA kit (Wako) according to the manufacturer's instructions. For detection of Arctic Aβ produced from the brains of $App^{NL\text{-}G\text{-}F}$ and $App^{G\text{-}F}$ mice, standard curves were drawn using human Aβ peptides carrying the Arctic mutation as described previously (*4*).

Verubecestat administration

Verubecestat (ChemScene) dissolved in PBS was administrated orally to 3-month-old mice using a flexible oral gavage needle (FUCHIGAMI) at a single dose of 10 mg/kg according to Kennedy *et al.* (*11*). Three hours after a single treatment, mouse brains were dissected and stored at −80°C.

Quantification and statistical analysis

All data are shown as the means ± SEM within each figure. For comparisons between two groups, data were analyzed by Student's *t* test, Welch's *t* test, or Mann-Whitney test. For comparisons among more than three groups, we used one-way analysis of variance (ANOVA) followed by Dunnett's post hoc analysis or Tukey's post hoc analysis. All statistical analysis were performed using GraphPad Prism 7 software (GraphPad software). The levels of statistical significance were presented as *P* values: $^{*}P < 0.05$, $^{**}P < 0.01$, and $^{***}P < 0.001$.

SUPPLEMENTARY MATERIALS

Supplementary material for this article is available at https://science.org/doi/10.1126/sciadv.abm6155

View/request a protocol for this paper from *Bio-protocol*.

REFERENCES AND NOTES

1. A. Alzheimer, R. A. Stelzmann, H. N. Schnitzlein, F. R. Murtagh, An English translation of Alzheimer's 1907 paper, "Uber eine eigenartige Erkankung der Hirnrinde". *Clin. Anat.* **8**, 429–431 (1995).
2. J. Sevigny, P. Chiao, T. Bussière, P. H. Weinreb, L. Williams, M. Maier, R. Dunstan, S. Salloway, T. Chen, Y. Ling, J. O'Gorman, F. Qian, M. Arastu, M. Li, S. Chollate, M. S. Brennan, O. Quintero-Monzon, R. H. Scannevin, H. M. Arnold, T. Engber, K. Rhodes, J. Ferrero, Y. Hang, A. Mikulskis, J. Grimm, C. Hock, R. M. Nitsch, A. Sandrock, The antibody aducanumab reduces Aβ plaques in Alzheimer's disease. *Nature* **537**, 50–56 (2016).
3. H. Sasaguri, P. Nilsson, S. Hashimoto, K. Nagata, T. Saito, B. de Strooper, J. Hardy, R. Vassar, B. Winblad, T. C. Saido, APP mouse models for Alzheimer's disease preclinical studies. *EMBO J.* **36**, 2473–2487 (2017).
4. T. Saito, Y. Matsuba, N. Mihira, J. Takano, P. Nilsson, S. Itohara, N. Iwata, T. C. Saido, Single App knock-in mouse models of Alzheimer's disease. *Nat. Neurosci.* **17**, 661–663 (2014).
5. S. Li, H. Hou, T. Mori, D. Sawmiller, A. Smith, J. Tian, Y. Wang, B. Giunta, P. R. Sanberg, S. Zhang, J. Tan, Swedish mutant APP-based BACE1 binding site peptide reduces APP β-cleavage and cerebral Aβ levels in Alzheimer's mice. *Sci. Rep.* **5**, 11322 (2015).
6. D. Kwart, A. Gregg, C. Scheckel, E. A. Murphy, D. Paquet, M. Duffield, J. Fak, O. Olsen, R. B. Darnell, M. Tessier-Lavigne, A large panel of isogenic APP and PSEN1 mutant human iPSC neurons reveals shared endosomal abnormalities mediated by APP β-CTFs, not Aβ. *Neuron* **104**, 256–270.e5 (2019).
7. I. Lauritzen, R. Pardossi-Piquard, A. Bourgeois, S. Pagnotta, M.-G. Biferi, M. Barkats, P. Lacor, W. Klein, C. Bauer, F. Checler, Intraneuronal aggregation of the β-CTF fragment of APP (C99) induces Aβ-independent lysosomal-autophagic pathology. *Acta Neuropathol.* **132**, 257–276 (2016).
8. J. E. Garneau, M.-È. Dupuis, M. Villion, D. A. Romero, R. Barrangou, P. Boyaval, C. Fremaux, P. Horvath, A. H. Magadán, S. Moineau, The CRISPR/Cas bacterial immune system cleaves bacteriophage and plasmid DNA. *Nature* **468**, 67–71 (2010).
9. A. C. Komor, A. H. Badran, D. R. Liu, CRISPR-based technologies for the manipulation of eukaryotic genomes. *Cell* **169**, 559 (2017).
10. J. D. Scott, S. W. Li, A. P. J. Brunskill, X. Chen, K. Cox, J. N. Cumming, M. Forman, E. J. Gilbert, R. A. Hodgson, L. A. Hyde, Q. Jiang, U. Iserloh, I. Kazakevich, R. Kuvelkar, H. Mei, J. Meredith, J. Misiaszek, P. Orth, L. M. Rossiter, M. Slater, J. Stone, C. O. Strickland, J. H. Voigt, G. Wang, H. Wang, Y. Wu, W. J. Greenlee, E. M. Parker, M. E. Kennedy, A. W. Stamford, Discovery of the 3-Imino-1,2,4-thiadiazinane 1,1-dioxide derivative verubecestat (MK-8931)-A β-site amyloid precursor protein cleaving enzyme 1 inhibitor for the treatment of Alzheimer's disease. *J. Med. Chem.* **59**, 10435–10450 (2016).
11. M. E. Kennedy, A. W. Stamford, X. Chen, K. Cox, J. N. Cumming, M. F. Dockendorf, M. Egan, L. Ereshefsky, R. A. Hodgson, L. A. Hyde, S. Jhee, H. J. Kleijn, R. Kuvelkar, W. Li, B. A. Mattson, H. Mei, J. Palcza, J. D. Scott, M. Tanen, M. D. Troyer, J. L. Tseng, J. A. Stone, E. M. Parker, M. S. Forman, The BACE1 inhibitor verubecestat (MK-8931) reduces CNS β-amyloid in animal models and in Alzheimer's disease patients. *Sci. Transl. Med.* **8**, 363ra150 (2016).
12. T. J. Cradick, P. Qiu, C. M. Lee, E. J. Fine, G. Bao, COSMID: A web-based tool for identifying and validating CRISPR/Cas off-target sites. *Mol. Ther. Nucleic Acids* **3**, e214 (2014).
13. S. Bae, J. Park, J. S. Kim, Cas-OFFinder: A fast and versatile algorithm that searches for potential off-target sites of Cas9 RNA-guided endonucleases. *Bioinformatics* **30**, 1473–1475 (2014).
14. H. Yamakawa, S. Yagishita, E. Futai, S. Ishiura, β-Secretase inhibitor potency is decreased by aberrant beta-cleavage location of the "Swedish mutant" amyloid precursor protein. *J. Biol. Chem.* **285**, 1634–1642 (2010).
15. I. Hussain, J. Hawkins, D. Harrison, C. Hille, G. Wayne, L. Cutler, T. Buck, D. Walter, E. Demont, C. Howes, A. Naylor, P. Jeffrey, M. I. Gonzalez, C. Dingwall, A. Michel, S. Redshaw, J. B. Davis, Oral administration of a potent and selective non-peptidic BACE-1 inhibitor decreases beta-cleavage of amyloid precursor protein and amyloid-beta production in vivo. *J. Neurochem.* **100**, 802–809 (2007).
16. S. Rabe, J. Reichwald, D. Ammaturo, B. de Strooper, P. Saftig, U. Neumann, M. Staufenbiel, The Swedish APP mutation alters the effect of genetically reduced BACE1 expression on the APP processing. *J. Neurochem.* **119**, 231–239 (2011).
17. H. Kalimo, M. Lalowski, N. Bogdanovic, O. Philipson, T. D. Bird, D. Nochlin, G. D. Schellenberg, R.-M. Brundin, T. Olofsson, R. Soliymani, M. Baumann, O. Wirths, T. A. Bayer, L. N. G. Nilsson, H. Basun, L. Lannfelt, M. Ingelsson, The Arctic AβPP mutation leads to Alzheimer's disease pathology with highly variable topographic deposition of differentially truncated Aβ. *Acta Neuropathol. Commun.* **1**, 60 (2013).
18. C. O. Y. Hung, F. J. Livesey, Altered γ-secretase processing of APP disrupts lysosome and autophagosome function in monogenic Alzheimer's disease. *Cell Rep.* **25**, 3647–3660.e2 (2018).
19. Y. Jiang, K. A. Mullaney, C. M. Peterhoff, S. Che, S. D. Schmidt, A. Boyer-Boiteau, S. D. Ginsberg, A. M. Cataldo, P. M. Mathews, R. A. Nixon, Alzheimer's-related endosome dysfunction in Down syndrome is Abeta-independent but requires APP and is reversed by BACE-1 inhibition. *Proc. Natl. Acad. Sci. U.S.A.* **107**, 1630–1635 (2010).

20. S. Kim, Y. Sato, P. S. Mohan, C. Peterhoff, A. Pensalfini, A. Rigoglioso, Y. Jiang, R. A. Nixon, Evidence that the rab5 effector APPL1 mediates APP-βCTF-induced dysfunction of endosomes in Down syndrome and Alzheimer's disease. *Mol. Psychiatry* **21**, 707–716 (2016).
21. G. Woodruff, S. M. Reyna, M. Dunlap, R. van der Kant, J. A. Callender, J. E. Young, E. A. Roberts, L. S. B. Goldstein, Defective transcytosis of APP and lipoproteins in human iPSC-derived neurons with familial Alzheimer's disease mutations. *Cell Rep.* **17**, 759–773 (2016).
22. W. Xu, A. M. Weissmiller, J. A. White II, F. Fang, X. Wang, Y. Wu, M. L. Pearn, X. Zhao, M. Sawa, S. Chen, S. Gunawardena, J. Ding, W. C. Mobley, C. Wu, Amyloid precursor protein-mediated endocytic pathway disruption induces axonal dysfunction and neurodegeneration. *J. Clin. Invest.* **126**, 1815–1833 (2016).
23. A. M. Cataldo, S. Petanceska, N. B. Terio, C. M. Peterhoff, R. Durham, M. Mercken, P. D. Mehta, J. Buxbaum, V. Haroutunian, R. A. Nixon, Abeta localization in abnormal endosomes: Association with earliest Abeta elevations in AD and Down syndrome. *Neurobiol. Aging* **25**, 1263–1272 (2004).
24. S. Treusch, S. Hamamichi, J. L. Goodman, K. E. S. Matlack, C. Y. Chung, V. Baru, J. M. Shulman, A. Parrado, B. J. Bevis, J. S. Valastyan, H. Han, M. Lindhagen-Persson, E. M. Reiman, D. A. Evans, D. A. Bennett, A. Olofsson, P. L. DeJager, R. E. Tanzi, K. A. Caldwell, G. A. Caldwell, S. Lindquist, Functional links between Aβ toxicity, endocytic trafficking, and Alzheimer's disease risk factors in yeast. *Science* **334**, 1241–1245 (2011).
25. K. Willén, J. R. Edgar, T. Hasegawa, N. Tanaka, C. E. Futter, G. K. Gouras, Aβ accumulation causes MVB enlargement and is modelled by dominant negative VPS4A. *Mol. Neurodegener.* **12**, 61 (2017).
26. K. E. Marshall, D. M. Vadukul, K. Staras, L. C. Serpell, Misfolded amyloid-β-42 impairs the endosomal-lysosomal pathway. *Cell. Mol. Life Sci.* **77**, 5031–5043 (2020).
27. D. Baglietto-Vargas, S. Forner, L. Cai, A. C. Martini, L. Trujillo-Estrada, V. Swarup, M. M. T. Nguyen, K. Do Huynh, D. I. Javonillo, K. M. Tran, J. Phan, S. Jiang, E. A. Kramár, C. Nuñez-Diaz, G. Balderrama-Gutierrez, F. Garcia, J. Childs, C. J. Rodriguez-Ortiz, J. A. Garcia-Leon, M. Kitazawa, M. Shahnawaz, D. P. Matheos, X. Ma, C. da Cunha, K. C. Walls, R. R. Ager, C. Soto, A. Gutierrez, I. Moreno-Gonzalez, A. Mortazavi, A. J. Tenner, G. R. MacGregor, M. Wood, K. N. Green, F. M. LaFerla, Generation of a humanized Aβ expressing mouse demonstrating aspects of Alzheimer's disease-like pathology. *Nat. Commun.* **12**, 2421 (2021).
28. A. Knupp, S. Mishra, R. Martinez, J. E. Braggin, M. Szabo, C. Kinoshita, D. W. Hailey, S. A. Small, S. Jayadev, J. E. Young, Depletion of the AD risk gene SORL1 selectively impairs neuronal endosomal traffic independent of amyloidogenic APP processing. *Cell Rep.* **31**, 107719 (2020).
29. A. Pensalfini, S. Kim, S. Subbanna, C. Bleiwas, C. N. Goulbourne, P. H. Stavrides, Y. Jiang, J.-H. Lee, S. Darji, M. Pawlik, C. Huo, J. Peddy, M. J. Berg, J. F. Smiley, B. S. Basavarajappa, R. A. Nixon, Endosomal dysfunction induced by directly overactivating Rab5 recapitulates prodromal and neurodegenerative features of Alzheimer's disease. *Cell Rep.* **33**, 108420 (2020).
30. T. Jonsson, J. K. Atwal, S. Steinberg, J. Snaedal, P. V. Jonsson, S. Bjornsson, H. Stefansson, P. Sulem, D. Gudbjartsson, J. Maloney, K. Hoyte, A. Gustafson, Y. Liu, Y. Lu, T. Bhangale, R. R. Graham, J. Huttenlocher, G. Bjornsdottir, O. A. Andreassen, E. G. Jönsson, A. Palotie, T. W. Behrens, O. T. Magnusson, A. Kong, U. Thorsteinsdottir, R. J. Watts, K. Stefansson, A mutation in APP protects against Alzheimer's disease and age-related cognitive decline. *Nature* **488**, 96–99 (2012).
31. A. B. Elvang, C. Volbracht, L. Ø. Pedersen, K. G. Jensen, J.-J. Karlsson, S. A. Larsen, A. Mørk, T. B. Stensbøl, J. F. Bastlund, Differential effects of gamma-secretase and BACE1 inhibition on brain Aβ levels in vitro and in vivo. *J. Neurochem.* **110**, 1377–1387 (2009).
32. P. D. Hsu, D. A. Scott, J. A. Weinstein, F. A. Ran, S. Konermann, V. Agarwala, Y. Li, E. J. Fine, X. Wu, O. Shalem, T. J. Cradick, L. A. Marraffini, G. Bao, F. Zhang, DNA targeting specificity of RNA-guided Cas9 nucleases. *Nat. Biotechnol.* **31**, 827–832 (2013).
33. H. Yang, H. Wang, R. Jaenisch, Generating genetically modified mice using CRISPR/Cas-mediated genome engineering. *Nat. Protoc.* **9**, 1956–1968 (2014).
34. T. C. Saido, T. Iwatsubo, D. M. Mann, H. Shimada, Y. Ihara, S. Kawashima, Dominant and differential deposition of distinct beta-amyloid peptide species, A beta N3(pE), in senile plaques. *Neuron* **14**, 457–466 (1995).

Acknowledgments: We thank N. Iwata (Nagasaki University) and A. Hoshino and T. Hino (Kyoto Prefectural University of Medicine) for valuable discussions. We also thank Y. Nagai-Watanabe for secretarial work. **Funding:** This work was supported by AMED under grant number JP20dm0207001 [Brain Mapping by Integrated Neurotechnologies for Disease Studies (Brain/MINDS)] (T.C.S.), JSPS KAKENHI grant number JP18K07402 (H.S.), and the Takeda Science Foundation (H.S.). **Author contributions**: N.W., K.S., K.N., T.S., T.C.S., and H.S. designed the research plan. N.W., K.S., G.S., A.I., N.K., M.T., N.M., M.S., N.Y., and R.F. performed the experiments. N.W., K.S., K.N., T.S., T.C.S., and H.S. analyzed and interpreted data. H.S., K.S., N.W., S.H., T.S., and T.C.S. wrote the manuscript together. H.S., T.O., T.S., and T.C.S. supervised the entire research. **Competing interests:** The authors declare that they have no competing interests. **Data and materials availability:** All data needed to evaluate the conclusions in the paper are present in the paper and/or the Supplementary Materials.

Submitted 29 September 2021
Accepted 22 April 2022
Published 8 June 2022
10.1126/sciadv.abm6155